First results in the search for Dark Sectors at NA64 with the CERN SPS high energy muon beam

Yu. M. Andreev,[1] D. Banerjee,[2] B. Banto Oberhauser,[3] J. Bernhard,[2] P. Bisio,[4, 5] N. Charitonidis,[2] P. Crivelli,[3, *] E. Depero,[3] A. V. Dermenev,[1] S. V. Donskov,[1] R. R. Dusaev,[1] T. Enik,[6] V. N. Frolov,[6] A. Gardikiotis,[7] S. V. Gertsenberger,[6] S. Girod,[2] S. N. Gninenko,[1, 8] M. Hösgen,[9] R. Joosten,[10] V. A. Kachanov,[1] Y. Kambar,[6] A. E. Karneyeu,[1] E. A. Kasianova,[6] G. Kekelidze,[6] B. Ketzer,[9] D. V. Kirpichnikov,[1] M. M. Kirsanov,[1] V. N. Kolosov,[1] V. A. Kramarenko,[1, 6] L. V. Kravchuk,[1] N. V. Krasnikov,[1, 6] S. V. Kuleshov,[8, 11] V. E. Lyubovitskij,[1, 12, 11] V. Lysan,[6] V. A. Matveev,[6] R. Mena Fredes,[11, 12] R. G. Mena Yanssen,[11, 12] L. Molina Bueno,[13, †] M. Mongillo,[3] D. V. Peshekhonov,[6] V. A. Polyakov,[1] B. Radics,[14] K. M. Salamatin,[6] V. D. Samoylenko,[1] D. A. Shchukin,[1] O. Soto,[15, 11] H. Sieber,[3, ‡] V. O. Tikhomirov,[1] I. V. Tlisova,[1] A. N. Toropin,[1] M. Tuzi,[13] M. B. Veit,[16] P. V. Volkov,[1, 6] V. Yu. Volkov,[1] I. V. Voronchikhin,[1] J. Zamora-Saá,[8, 11] and A. S. Zhevlakov[6]

[1]Authors affiliated with an institute covered by a cooperation agreement with CERN
[2]CERN, European Organization for Nuclear Research, CH-1211 Geneva, Switzerland
[3]ETH Zürich, Institute for Particle Physics and Astrophysics, CH-8093 Zürich, Switzerland
[4]INFN, Sezione di Genova, 16147 Genova, Italia
[5]Università degli Studi di Genova, 16126 Genova, Italia
[6]Authors affiliated with an international laboratory covered by a cooperation agreement with CERN
[7]Physics Department, University of Patras, 265 04 Patras, Greece
[8]Center for Theoretical and Experimental Particle Physics, Facultad de Ciencias Exactas, Universidad Andres Bello, Fernandez Concha 700, Santiago, Chile
[9]Universität Bonn, Helmholtz-Institut für Strahlen-und Kernphysik, 53115 Bonn, Germany
[10]Rheinische Friedrich-Wilhelms-Universität, Bonn, Germany
[11]Millennium Institute for Subatomic Physics at High-Energy Frontier (SAPHIR), Fernandez Concha 700, Santiago, Chile
[12]Universidad Técnica Federico Santa María and CCTVal, 2390123 Valparaíso, Chile
[13]Instituto de Fisica Corpuscular (CSIC/UV), Carrer del Catedratic Jose Beltran Martinez, 2, 46980 Paterna, Valencia, Spain
[14]York University, Toronto, Canada
[15]Departamento de Fisica, Facultad de Ciencias, Universidad de La Serena, Avenida Cisternas 1200, La Serena, Chile
[16]Johannes Gutenberg Universitaet Mainz, Germany
(Dated: April 3, 2024)

We report the first search for Dark Sectors performed at the NA64 experiment employing a high energy muon beam and a missing energy-momentum technique. Muons from the M2 beamline at the CERN Super Proton Synchrotron with a momentum of 160 GeV/c are directed to an active target. The signal signature consists of a single scattered muon with momentum < 80 GeV/c in the final state, accompanied by missing energy, i.e. no detectable activity in the downstream calorimeters. For a total data set of $(1.98 \pm 0.02) \times 10^{10}$ muons on target, no event is observed in the expected signal region. This allows us to set new limits on the remaining $(m_{Z'}, g_{Z'})$ parameter space of a new Z' $(L_\mu - L_\tau)$ vector boson which could explain the muon $(g - 2)_\mu$ anomaly. Additionally, our study excludes part of the parameter space suggested by the thermal Dark Matter relic abundance. Our results pave the way to explore Dark Sectors and light Dark Matter with muon beams in a unique and complementary way to other experiments.

In this Letter, we present the first results of the NA64 experiment muon program, dubbed NA64μ, employing a novel missing energy-momentum technique to look for sub-GeV gauge bosons coupled to muons [1]. Dark Sectors (DS) are a promising paradigm to address open questions of the Standard Model (SM) such as the origin of Dark Matter (DM) [2]. In this framework, one postulates a new sector of particles below the electroweak scale that are not charged under the SM but could have a phenomenology of their own [3–8]. In addition to gravity, the interactions between DS states and the SM could proceed through portal mediators. If one assumes that DM is made of the lightest stable DS particles, the resulting feeble interaction between the two sectors can be compatible with cosmological observations and, thus, would accommodate a solution to the DM problem [9–12]. DS models became an extremely fertile domain of exploration with many different techniques tackling the very large parameter space of possible DM candidates (see e.g. for recent reviews [13–16]). From the broad DS landscape, many scenarios suggest new feeble interactions with muons mediated by scalar, pseudoscalar or vector-like particles. The new feebly interacting mediator, X, could be produced in the bremsstrahlung-like reaction of 160 GeV/c muons with a target (N) followed by its subsequent invisible decay, $\mu N \to \mu N X$; $X \to$ invisible (see Fig. 1).
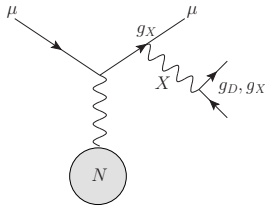
Figure 1. Production of a generic X boson through a bremsstrahlung-like reaction, followed by its prompt invisible decay, $\mu N \to \mu N X$; $X \to$ invisible. The interaction strength of the X boson with SM particles and DM candidates is regulated by the couplings g_X and g_D respectively. The nucleus is assumed to recoil elastically leaving only the outgoing muon and invisible energy in the detector.

Even though our results are model-independent, to demonstrate the potential of our experiment to search for DS, we use as a benchmark scenario a new sub-GeV Z' $L_\mu - L_\tau$ boson arising by gauging the difference of the lepton number between the muon and tau flavour. Interestingly, this model could explain the origin of DM and,

at the same time, the long-standing $g - 2$ muon anomaly in terms of new physics [17]. The current bounds for $m_{Z'} > 2m_\mu$ arise from direct searches, sensitive to the kinematically allowed visible decay channel $Z' \to \mu^+\mu^-$ [18–21]. Neutrino scattering experiments [22, 23] and missing energy searches through $Z' \to \bar{\chi}\chi$ [24, 25] provide constraints for $m_{Z'} < 2m_\mu$. The lower bound is set through the Z' contribution to the radiation density of the Universe through ΔN_{eff}, with its value being defined from both the CMB spectrum [12] and Big Bang nucleosynthesis (BBN) [21, 26, 27] to $m_{Z'} > 3 - 10$ MeV [28] and $g_{Z'} \sim 10^{-4} - 10^{-3}$. If a Z' boson exists, it could be produced in the reaction depicted in Fig. 1, $\mu N \to \mu N Z'$; $Z' \to$ invisible. In the *vanilla* model, the Z' can only decay to neutrinos, $Z' \to \bar{\nu}\nu$, while in extended models, it can additionally decay to DM candidates, $Z' \to \bar{\chi}\chi$, [29–31]. For a value of $g_\chi = 5 \times 10^{-2}$ one can accommodate in the same parameter space the muon $g - 2$ and the DM relic prediction [32]. For a viable DM candidate (below $m_\chi < 1$ GeV) $g_\chi \gg g_{Z'}$, the branching ratio to DS invisible final states can be assumed to be $\text{Br}(Z' \to \bar{\chi}\chi) \simeq 1$, while the ones in visible states $(Z' \to \mu^+\mu^-)$ and neutrinos can be neglected.
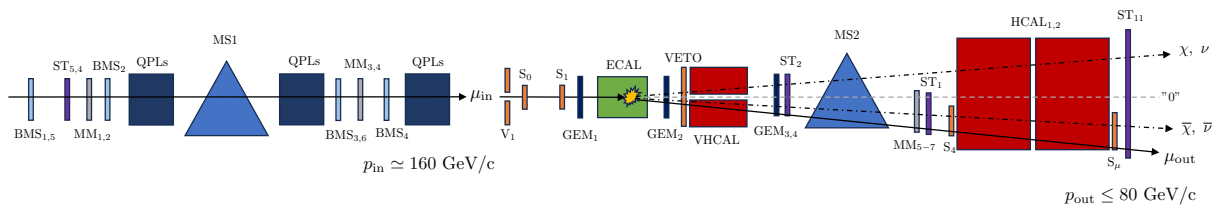

Figure 2. Schematic illustration of the NA64μ set-up and of a signal event topology. Well-defined incoming muons with momentum $p_{\text{in}} \simeq 160$ GeV/c are reconstructed in the first magnet spectrometer and tagged by a set of scintillator counters before arriving at the active target (ECAL). In the collision of muons with the target nuclei the bremsstrahlung-like reaction and subsequent invisible decay, $\mu N \to \mu N(Z' \to$ invisible) is produced. The resulting scattered muon with momentum $p_{\text{out}} \leq 80$ GeV/c is measured in the second spectrometer (MS2).

The search for signal events in NA64μ consists of the detection of a primary beam muon with a momentum of 160 GeV/c in the initial state and a single muon that scatters off the active target with missing momentum > 80 GeV/c in the final state, accompanied by missing energy, i.e. no detectable electromagnetic or hadronic activity in the downstream calorimeters. The working principle and experimental set-up are schematically shown in Fig. 2. The 160 GeV/c muons are delivered by the M2 beamline at the CERN Super Proton Synchrotron (SPS) accelerator [33]. The beam optics comprises a series of quadrupoles (QPLs) focusing the beam before the target with a divergency $\sigma_x \sim 0.9$ and $\sigma_y \sim 1.9$ cm [34]. The incoming muon momentum is reconstructed through a magnetic spectrometer (MS1) consisting of three 5 T·m bending magnets, together with

four 8×8 cm^2 micro-mesh gas detectors (Micromegas, MM$_{1-4}$), two 20×20 cm^2 straw tubes chambers (ST$_{5,4}$) and six variable-sized scintillator (Sc) hodoscopes, the beam momentum stations (BMS$_{1-6}$). The obtained momentum resolution is $\sigma_{p_{\text{in}}}/p_{\text{in}} \simeq 3.8\%$. The target is an active electromagnetic calorimeter (ECAL) composed of Shashlik-type modules made of lead-scintillator layers resulting in 40 radiation lengths (X_0). The ECAL has an asymmetric 5×6 lateral segmentation and a resolution of $\sigma_E/E = 8\%/\sqrt{E} \bigoplus 1\%$. The target is followed by a large 55×55 cm^2 high-efficiency veto counter (VETO) and a 5 nuclear interaction lengths (λ_{int}) copper-scintillator hadronic calorimeter (VHCAL) with a hole in its middle. The outgoing muon momentum is reconstructed through a second magnetic spectrometer consisting of a single 1.4 T·m bending magnet (MS2) together with

four 10×10 cm^2 gaseous electron multiplier trackers (GEM$_{1-4}$), two additional straw chambers (ST$_{2,1}$) and three 25×8 cm^2 Micromegas (MM$_{5-7}$) yielding a resolution of $\sigma_{p_{\text{out}}}/p_{\text{out}} \simeq 4.4\%$. To identify and remove any residuals from interactions in the detectors upstream of MS2 and ensure maximal hermeticity, two large 120×60 cm^2, $\lambda_{\text{int}} \simeq 30$ iron-Sc HCAL modules (HCAL$_{1,2}$), with energy resolution $\sigma_E/E = 65\%/\sqrt{E} + 6\%$, are placed at the end of the set-up together with a 120×60 cm^2 straw tube chamber, ST$_{11}$. Further details about calorimeters and tracking detectors can be found in [35] and in [36].

The trigger system is defined by a veto counter with a hole (V$_1$) and a set of 42 mm diameter plastic scintillators counters (S$_{0-1}$) before the target, together with two 20×20 cm^2 and 30×30 cm^2 counters (S$_4$ and S$_\mu$) sandwiching the HCAL modules, shifted from the undeflected beam axis (referred to as *zero-line*) to detect the scattered muons. The data were collected in two trigger configurations (S$_0 \times$S$_1 \times \overline{V_1} \times$S$_4 \times$S$_\mu$) with different S$_4$ and S$_\mu$ distances to the zero-line along the deflection axis $\hat{x}$, namely S$_\mu \hat{x} = -152$ mm and S$_\mu \hat{x} = -117$ mm with a similar S$_4 \hat{x} = -65$ mm. The corresponding measured rate is 0.04% and 0.07% of the calibration trigger (S$_{0,1} \times \overline{V_1}$) coincidences at a beam intensity of 2.8×10^6 μ/spill. In each configuration, we recorded respectively $(11.7 \pm 0.1) \times 10^9$ and $(8.1 \pm 0.1) \times 10^9$ muons on target (MOT) yielding a total accumulated data set of $(1.98 \pm 0.02) \times 10^{10}$ MOT.

A detailed `GEANT4` [37, 38] Monte Carlo (MC) simulation is performed to study the main background sources and the response of the detectors and the muon propagation. In the latter case, the full beam optics developed by the CERN BE-EA beam department is encompassed in the simulation framework using separately both the `TRANSPORT`, `HALO` and `TURTLE` programs [39–41], as well the `GEANT4` compatible beam delivery simulation (`BDSIM`) program [42–44] to simulate secondaries interactions in the beamline material. The signal acceptance is carefully studied using the `GEANT4` interface `DMG4` package [45, 46], including light mediators production cross-sections computations through muon bremsstrahlung [31]. The placements of S$_4$ and S$_\mu$ are optimized to compensate for the low signal yield at high masses, $\sigma_{Z'} \sim g_{Z'}^2 \alpha Z^2/m_{Z'}^2$, with α the fine structure constant and Z the atomic number of the target, through the angular acceptance being maximized for a scattered muon angle $\psi'_\mu \sim 10^{-2}$ rad after the ECAL. In addition, the trigger counters downstream of MS2 account for the expected 160 GeV/c mean deflected position at the level of S$_4$, estimated at $\langle \delta x \rangle \simeq -12.0$ mm from a detailed `GenFit`-based [47, 48] Runge-Kutta extrapolation scheme.

The signal region, $p_{\text{out}}^{\text{cut}} \leq 80$ GeV/c and $E_{\text{CAL}}^{\text{cut}} < 12$ GeV, is optimized with signal simulations and data-driven background estimations to maximize the sensitivity. The cut on the total energy deposit in the calorimeters, $E_{\text{CAL}}^{\text{cut}}$, is defined by fitting the minimum ionizing

particle (MIP) spectra obtained from the sum of the energy deposit in the ECAL, VHCAL and HCAL modules.

To minimize the background, the following set of selection criteria is used. (i) The incoming momentum should be in the momentum range 160 ± 20 GeV/c. (ii) A single track is reconstructed in each magnetic spectrometer (MS1 and MS2) to ensure that a single muon traverses the full set-up. (iii) At most one hit is reconstructed in MM$_{5-7}$ and ST$_1$ (no multiple hits) and the corresponding extrapolated track to the HCAL face is compatible with a MIP energy deposit in the expected cell. This cut verifies that no energetic enough secondaries from interactions upstream of MS2 arrive at the HCAL. (vi) The energy deposit in the calorimeters and the veto should be compatible with a MIP. This cut enforces the selection of events with no muon nuclear interactions in the calorimeters. The aforementioned cut-flow is applied to events distributed in the outgoing muon momentum and total energy deposit plane, (p_{out}, E_{CAL}), as shown in Fig. 3.
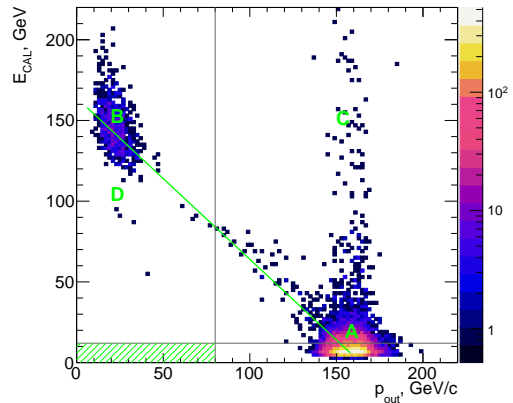

Figure 3. Event distribution in the (p_{out}, E_{CAL}) plane before the MIP-compatible requirement selection criterion. The signal region is defined as the shaded green rectangular area and the controlled region labeled with A through D (see text).

Region A is inherent to events with MIP-compatible energy deposits in all of the calorimeters, resulting in $p_{\text{in}} \simeq p_{\text{out}} \simeq 160$ GeV/c. By design, most unscattered beam muons do not pass through the S$_4$ and S$_\mu$ counters, however, the trigger condition can be fulfilled by sufficiently energetic residual ionization $\mu N \rightarrow \mu N + \delta e$ originating from the downstream trackers MM$_{5-7}$ or last HCAL$_2$ layers. The accumulation of events in region C is associated with large energy deposition of the full-momentum scattered muon in the HCAL, while region B corresponds to a hard scattering/bremsstrahlung in the ECAL, with a soft outgoing muon and full energy deposition in either the active target or HCAL. The small number of events between $p_{\text{out}} \geq 50$ GeV/c and $p_{\text{out}} \leq 100$ GeV/c are associated with hard muon bremsstrahlung

events, $\mu N \rightarrow \mu N + \gamma$, with $\psi'_\mu \ll 10^{-2}$ rad, as a result of the trigger optimization for signal events emitted at larger angles. The events in the region D are associated with muon nuclear interactions in the ECAL, $\mu N \rightarrow \mu + X$, with X containing any combination of π's, K, p, n..., with low-energy charged hadrons being deflected away in MS2, going out of the detector acceptance (typically the HCAL modules).

Background source	Background, n_b
(I) Momentum mis-reconstruction	0.05 ± 0.03
(II) $K \rightarrow \mu + \nu$, ... in-flight decays	0.010 ± 0.001
(III) Calorimeter non-hermeticity	< 0.01
Total n_b (conservatively)	0.07 ± 0.03

Table I. Expected main background level within the signal region, together with its statistical error, for the accumulated data set of $\sim 2 \times 10^{10}$ MOT.

An exhaustive discussion of background sources is given in [34, 49]. The main processes are summarised in Table I, with the dominant background contribution being associated with (I) momentum mis-reconstruction of the scattered muon in MS2. An incoming muon with 160 GeV/c is reconstructed after the target with momentum ≤ 80 GeV/c, whereas it truly is 160 GeV/c. This background is evaluated from data by selecting a sample of muons with $p_{\text{in}} = 160 \pm 2\sigma_{p_{\text{in}}}$ GeV/c measured in MS1, and a MIP-compatible energy deposit in the ECAL. The tails of the measured momentum distribution in MS2, p_{out}, are then extrapolated to the blinded signal region at 80 GeV/c to estimate the number of expected background events. The second most important background process is (II) kaon decays to (semi-)leptonic final states with muons, $K \rightarrow \mu\nu$, ..., before the ECAL target. Because of the level of hadron contamination in the M2 beamline, $P_h \simeq 5 \times 10^{-5}$ [33], incoming kaons could be reconstructed through MS1 with a momentum passing the selection criterion (i) and subsequently decaying to muons with energy ≤ 80 GeV, with the neutrino carrying away the remaining energy. This contribution is estimated from MC with the hadron contamination being extracted from existing data [33]. Pion decays do not contribute to this background, since due to kinematics, the muon momentum is always ≥ 80 GeV. Another background source is associated with (III) non-hermeticity in the calorimeters due to muon nuclear interactions in the target. As such, a leading hadron with energy $E_h \geq 80$ GeV could be produced and escape the ECAL with lesser energetic charged secondaries and the scattered muon. Because of the non-zero charge of the particles and the trigger acceptance, low-energy secondaries are deflected away through MS2 resulting in missing energy events. This background is extrapolated to the signal region from region D of Fig. 3. After applying all selection criteria

(i-iv) and summing up the processes contributing to the background, the expected background level is found to be 0.07 ± 0.03 for the total data set of $\sim 2 \times 10^{10}$ MOT.

The upper limits on the coupling $g_{Z'}$ as a function of its mass $m_{Z'}$ are estimated at 90% confidence level (CL) following the modified frequentist approach. In particular, the RooFit/RooStats-based [50–52] profile likelihood ratio statistical test is used in the asymptotic approximation [53]. The total number of signal events falling within the signal region is given by the sum of the two trigger configurations t

$$N_{Z'} = \sum_{t=1,2} N_{Z'}^t = \sum_{t=1,2} N_{\text{MOT}}^t \times \epsilon_{Z'}^t \times N_{Z'}^t(m_{Z'}, g_{Z'}), \tag{1}$$

where N_{MOT}^t is the number of MOT for trigger configuration t, $N_{Z'}^t$ the number of signals per MOT produced in the ECAL target, depending on the mass/coupling parameters $m_{Z'}$ and $g_{Z'}$, and $\epsilon_{Z'}^t$ the trigger-dependent signal efficiency.

The main systematic effects contributing to the signal yield defined in Eq. (1) are studied in detail. The uncertainty on N_{MOT}^t is conservatively set to 1%. The systematics associated with the Z' production cross-section are extracted from the uncertainty introduced by the Weiszäcker-Williams (WW) approximation and from QED corrections to the exact tree-level (ETL) expression. In the former case, the relative error in assessing the number of produced Z' ($N_{Z'}^t$) is found to be 2% [30, 31]. In the latter case both the running of α at the upper bound $Q^2 \simeq m_{Z'} \sim \mathcal{O}(1)$ GeV and higher order corrections from soft photon emissions, are estimated to contribute through respectively $\Delta N_{Z'} \sim \alpha^2 g_{Z'}^2 Z^2$ and through the Sudakov factor $\Delta N_{\text{soft}} \sim \exp(-\alpha/\pi)$ at the level of 2.4% and 1.4%. Uncertainties relative to the lead purity of the ECAL target are addressed at the level of 1%. The systematics on $\epsilon_{Z'}^t$ are evaluated by comparing the detector responses in MC and data around the MIP-compatible peak, in particular in the ECAL and HCAL. Through comparisons between spectra integration and the corresponding peak ratio, it is found that the related cumulative uncertainty does not exceed 4%. Because of the strong dependence of the efficiency $\epsilon_{Z'}^t$ on the trigger configuration t, in particular on the distance from the zero-line, additional uncertainties due to S4 and S$_\mu$ misalignment are studied through the change in efficiency as a response to small displacements of the Sc counters. Because of the $m_{Z'}$ mass-dependence of the trigger rate [34], the resulting uncertainty reaches up to $\leq 5\%$. As such the total systematic in the signal yield of Eq. (1) is $\leq 8\%$. The acceptance loss due to accidentals (pile-up events, $\sim 13\%$) entering the trigger time window is taken into account in the final efficiency computations. The signal efficiency peaks at its maximum of $\sim 12\%$ for the mass range $\mathcal{O}(100 \text{ MeV} - 1 \text{ GeV})$.

After unblinding, no event compatible with Z' produc-

tion is found in the signal region. This allows us to set the 90% CL exclusion limits on $g_{Z'}$ which are plotted in Fig. 4, left, in the $(m_{Z'}, g_{Z'})$ parameter space, together with the values of Δa_μ compatible with the muon $g - 2$ anomaly, within $\pm 2\sigma$. The band is computed using the latest results of the Muon $g - 2$ collaboration, $a_\mu(\text{Exp}) = 116\,592\,059(22) \times 10^{-11}$ [54] and the SM prediction of $a_\mu(\text{SM}) = 116\,591\,810(43) \times 10^{-11}$ from the Muon $g - 2$ Theory Initiative (TI) [55]. It is worth noting that the extraction of the hadronic vacuum polarization contribution using the latest results from the CMD-3 collaboration [56, 57] disagree within the 2.5-5σ level with the TI value. Note that the recent lattice QCD computations from the BMW collaboration [58] are also in tension with the TI value by 2.1σ.

Our results, excluding a previously unexplored parameter space with masses $m_{Z'} \gtrsim 40$ MeV and cou-

pling $g_{Z'} \gtrsim 5 \times 10^{-4}$, are the first search for a light Z' (vanilla $L_\mu - L_\tau$ model) with a muon beam using the missing energy-momentum technique (see Fig. 4, left). Figure 4, right, shows the obtained limits at 90% CL in the target parameter space (m_χ, y) with freeze-out parameter $y = (g_\chi g_{Z'})^2 (m_\chi/m_{Z'})^4$ for accelerator-based experiments probing thermal DM for $m_{Z'} = 3m_\chi$, away from the resonant enhancement $m_{Z'} \simeq 2m_\chi$, and $g_\chi = 5 \times 10^{-2}$. The thermal targets for favored y values are plotted for scalar, pseudo-Dirac, and Majorana DM candidate scenarios, and obtained from the integration of the underlying Boltzmann equation [59]. The results indicate that NA64μ excludes a portion of the (m_χ, y) parameter space, below the current CCFR [22, 60] limits, constraining for a choice of masses $m_\chi \lesssim 40$ MeV the dimensionless parameter to $y \lesssim 6 \times 10^{-12}$.
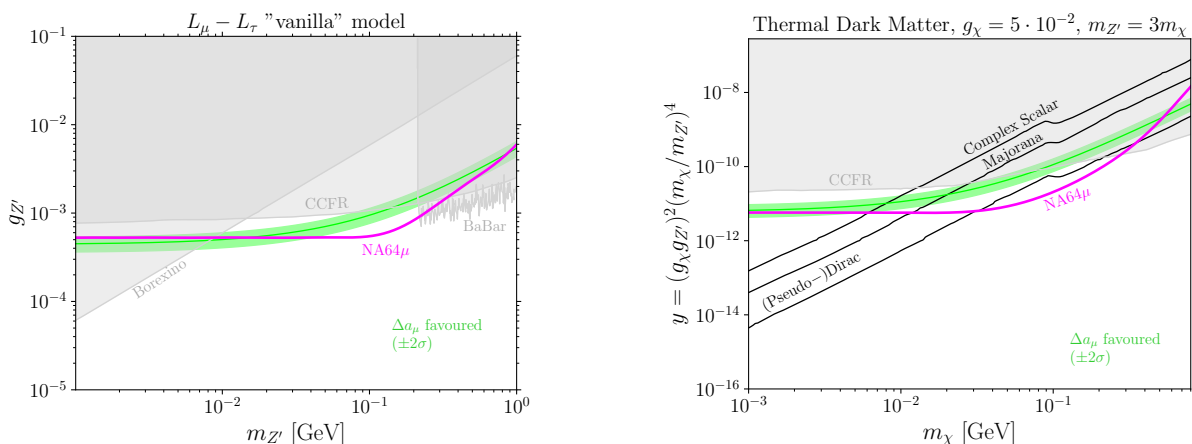

Figure 4. Left: NA64μ 90% CL exclusion limits on the coupling $g_{Z'}$ as a function of the Z' mass, $m_{Z'}$, for the vanilla $L_\mu - L_\tau$ model. The $\pm 2\sigma$ band for the Z' contribution to the $(g - 2)_\mu$ discrepancy is also shown. Existing constraints from BaBar [61, 62] and from neutrino experiments such as BOREXINO [21, 63, 64] and CCFR [22, 60] are plotted. Right: The 90% CL exclusion limits obtained by the NA64μ experiment in the (m_χ, y) parameters space for thermal Dark Matter charged under $U(1)_{L_\mu - L_\tau}$ with $m_{Z'} = 3m_\chi$ and the coupling $g_\chi = 5 \times 10^{-2}$ for 2×10^{10} MOT. The branching ratio to invisible final states is assumed to be Br($Z' \to$ invisible) $\simeq 1$ (see text for details). Existing bounds obtained through the CCFR experiment [22, 60] are shown for completeness. The thermal targets for the different scenarios are taken from [59].

In summary, for a data set of $(1.98 \pm 0.02) \times 10^{10}$ MOT, no event falling within the expected signal region is observed. Therefore, 90% CL upper limits are set in the $(m_{Z'}, g_{Z'})$ parameter space of the $L_\mu - L_\tau$ vanilla model, constraining viable mass values for the explanation of the $(g - 2)_\mu$ anomaly to $6 - 7$ MeV $\lesssim m_{Z'} \lesssim 40$ MeV, with $g_{Z'} \lesssim 6 \times 10^{-4}$. New constraints on light thermal DM for values $y \gtrsim 6 \times 10^{-12}$ for $m_\chi \gtrsim 40$ MeV are also obtained. The use of a muon beam demonstrated in this work opens a new window to explore other well-motivated scenarios such as benchmark dark photon models in the mass region $(0.1 - 1)$ GeV [65], scalar portals [31], millicharged

particles [66] or $\mu \to e$ or $\mu \to \tau$ processes involving Lepton Flavour Conversion [67–69], complementing the DS quest world wide effort [13–16]. Improvements in the experimental set-up such as: an additional magnetic spectrometer to reduce by more than an order of magnitude the background from momentum mis-reconstruction, and new detectors able to cope with rates up to $10^8 \mu$/spill available at the SPS M2 beamline, would allow NA64μ to collect up to three orders of magnitude more data. With such statistics, NA64μ can probe unequivocally a variety of muon-philic DS scenarios complementing present experiments such as Belle-II [25] or FASER [70], and future

projects as M^3 [32].

* **e-mail**:paolo.crivelli@cern.ch
† **e-mail**:laura.molina.bueno@cern.ch
‡ **e-mail**:henri.hugo.sieber@cern.ch

[1] S. N. Gninenko *et al.*, CERN-SPSC-2018-024, SPSC-P-348-ADD-3 (2018).

[2] J. L. Feng, Ann. Rev. Astron. Astrophys. **48**, 495 (2010), arXiv:1003.0904 [astro-ph.CO].

[3] N. Arkani-Hamed, D. P. Finkbeiner, T. R. Slatyer, and N. Weiner, Phys. Rev. D **79**, 015014 (2009), arXiv:0810.0713 [hep-ph].

[4] M. Pospelov and A. Ritz, Phys. Lett. B **671**, 391 (2009), arXiv:0810.1502 [hep-ph].

[5] D. Hooper, N. Weiner, and W. Xue, Phys. Rev. D **86**, 056009 (2012), arXiv:1206.2929 [hep-ph].

[6] M. Pospelov, A. Ritz, and M. B. Voloshin, Phys. Lett. B **662**, 53 (2008), arXiv:0711.4866 [hep-ph].

[7] M. Pospelov, Phys. Rev. D **80**, 095002 (2009), arXiv:0811.1030 [hep-ph].

[8] R. Essig *et al.*, in *Community Summer Study 2013: Snowmass on the Mississippi* (2013) arXiv:1311.0029 [hep-ph].

[9] J. L. Feng, H. Tu, and H.-B. Yu, JCAP **10**, 043 (2008), arXiv:0808.2318 [hep-ph].

[10] J. L. Feng and J. Kumar, Phys. Rev. Lett. **101**, 231301 (2008), arXiv:0803.4196 [hep-ph].

[11] G. Arcadi, M. Dutra, P. Ghosh, M. Lindner, Y. Mambrini, M. Pierre, S. Profumo, and F. S. Queiroz, Eur. Phys. J. C **78**, 203 (2018), arXiv:1703.07364 [hep-ph].

[12] N. Aghanim *et al.* (Planck), Astron. Astrophys. **641**, A6 (2020), [Erratum: Astron.Astrophys. 652, C4 (2021)], arXiv:1807.06209 [astro-ph.CO].

[13] J. Jaeckel, M. Lamont, and C. Vallée, Nature Phys. **16**, 393 (2020).

[14] G. Lanfranchi, M. Pospelov, and P. Schuster, Ann. Rev. Nucl. Part. Sci. **71**, 279 (2021), arXiv:2011.02157 [hep-ph].

[15] G. Krnjaic *et al.*, (2022), arXiv:2207.00597 [hep-ph].

[16] C. Antel *et al.*, in *Workshop on Feebly-Interacting Particles* (2023) arXiv:2305.01715 [hep-ph].

[17] I. Holst, D. Hooper, and G. Krnjaic, Phys. Rev. Lett. **128**, 141802 (2022), arXiv:2107.09067 [hep-ph].

[18] J. P. Lees *et al.* (BaBar), Phys. Rev. D **94**, 011102 (2016), arXiv:1606.03501 [hep-ex].

[19] A. M. Sirunyan *et al.* (CMS), Phys. Lett. B **792**, 345 (2019), arXiv:1808.03684 [hep-ex].

[20] G. Aad *et al.* (ATLAS), JHEP **07**, 090 (2023), arXiv:2301.09342 [hep-ex].

[21] A. Kamada and H.-B. Yu, Phys. Rev. D **92**, 113004 (2015), arXiv:1504.00711 [hep-ph].

[22] S. R. Mishra *et al.* (CCFR), Phys. Rev. Lett. **66**, 3117 (1991).

[23] D. Geiregat *et al.* (CHARM-II), Phys. Lett. B **245**, 271 (1990).

[24] Y. M. Andreev *et al.* (NA64), Phys. Rev. D **106**, 032015 (2022), arXiv:2206.03101 [hep-ex].

[25] I. Adachi *et al.* (Belle-II), Phys. Rev. Lett. **130**, 231801 (2023), arXiv:2212.03066 [hep-ex].

[26] B. Ahlgren, T. Ohlsson, and S. Zhou, Phys. Rev. Lett. **111**, 199001 (2013), arXiv:1309.0991 [hep-ph].

[27] M. Escudero, D. Hooper, G. Krnjaic, and M. Pierre, JHEP **03**, 071 (2019), arXiv:1901.02010 [hep-ph].

[28] N. Sabti, J. Alvey, M. Escudero, M. Fairbairn, and D. Blas, JCAP **01**, 004 (2020), arXiv:1910.01649 [hep-ph].

[29] S. N. Gninenko, D. V. Kirpichnikov, M. M. Kirsanov, and N. V. Krasnikov, Phys. Lett. B **782**, 406 (2018), arXiv:1712.05706 [hep-ph].

[30] D. V. Kirpichnikov, H. Sieber, L. M. Bueno, P. Crivelli, and M. M. Kirsanov, Phys. Rev. D **104**, 076012 (2021), arXiv:2107.13297 [hep-ph].

[31] H. Sieber, D. V. Kirpichnikov, I. V. Voronchikhin, P. Crivelli, S. N. Gninenko, M. M. Kirsanov, N. V. Krasnikov, L. Molina-Bueno, and S. K. Sekatskii, Phys. Rev. D **108**, 056018 (2023), arXiv:2305.09015 [hep-ph].

[32] Y. Kahn, G. Krnjaic, N. Tran, and A. Whitbeck, JHEP **09**, 153 (2018), arXiv:1804.03144 [hep-ph].

[33] N. Doble, L. Gatignon, G. von Holtey, and F. Novoskoltsev, Nucl. Instrum. Meth. A **343**, 351 (1994).

[34] H. Sieber, D. Banerjee, P. Crivelli, E. Depero, S. N. Gninenko, D. V. Kirpichnikov, M. M. Kirsanov, V. Poliakov, and L. Molina Bueno, Phys. Rev. D **105**, 052006 (2022), arXiv:2110.15111 [hep-ex].

[35] D. Banerjee *et al.* (NA64), Phys. Rev. D **97**, 072002 (2018), arXiv:1710.00971 [hep-ex].

[36] D. Banerjee *et al.*, Nucl. Instrum. Meth. A **881**, 72 (2018), arXiv:1708.04087 [physics.ins-det].

[37] S. Agostinelli *et al.* (GEANT4), Nucl. Instrum. Meth. A **506**, 250 (2003).

[38] J. Allison *et al.*, Nucl. Instrum. Meth. A **835**, 186 (2016).

[39] K. L. Brown, F. Rothacker, D. C. Carey, and F. C. Iselin, (1983), 10.5170/CERN-1980-004.

[40] C. Iselin, (1974), 10.5170/CERN-1974-017.

[41] K. L. Brown and F. C. Iselin, (1974), 10.5170/CERN-1974-002.

[42] L. J. Nevay *et al.*, Comput. Phys. Commun. **252**, 107200 (2020), arXiv:1808.10745 [physics.comp-ph].

[43] L. J. Nevay, A. Abramov, S. T. Boogert, *et al.*, CERN Yellow Rep. Conf. Proc. **2**, 45 (2020).

[44] L. J. Nevay, A. Abramov, J. Albrecht, *et al.*, in *10th International Particle Accelerator Conference* (2019) p. WEPTS058.

[45] M. Bondi, A. Celentano, R. R. Dusaev, D. V. Kirpichnikov, M. M. Kirsanov, N. V. Krasnikov, L. Marsicano, and D. Shchukin, Comput. Phys. Commun. **269**, 108129 (2021), arXiv:2101.12192 [hep-ph].

[46] B. B. Oberhauser *et al.*, (2024), arXiv:2401.12573 [hep-ph].

[47] J. Rauch and T. Schlüter, J. Phys. Conf. Ser. **608**, 012042 (2015), arXiv:1410.3698 [physics.ins-det].

[48] T. Bilka *et al.*, (2019), arXiv:1902.04405 [physics.data-an].

[49] S. Gninenko (NA64 Collaboration), *Addendum to the Proposal P348: Search for dark sector particles weakly coupled to muon with NA64μ*, Tech. Rep. (CERN, Geneva, 2018).

[50] W. Verkerke and D. P. Kirkby, eConf **C0303241**, MOLT007 (2003), arXiv:physics/0306116.

[51] Z. Wolffs, P. Bos, C. Burgard, E. Michalainas, L. Moneta, J. Rembser, and W. Verkerke, PoS **ICHEP2022**, 249 (2022).

[52] L. Moneta, K. Belasco, K. S. Cranmer, S. Kreiss, A. Lazzaro, D. Piparo, G. Schott, W. Verkerke, and M. Wolf, PoS **ACAT2010**, 057 (2010), arXiv:1009.1003 [physics.data-an].

[53] G. Cowan, K. Cranmer, E. Gross, and O. Vitells, Eur. Phys. J. C **71**, 1554 (2011), [Erratum: Eur.Phys.J.C 73, 2501 (2013)], arXiv:1007.1727 [physics.data-an].

[54] D. P. Aguillard *et al.* (Muon g-2), Phys. Rev. Lett. **131**, 161802 (2023), arXiv:2308.06230 [hep-ex].

[55] T. Aoyama *et al.*, Phys. Rept. **887**, 1 (2020), arXiv:2006.04822 [hep-ph].

[56] F. V. Ignatov *et al.* (CMD-3), (2023), arXiv:2302.08834 [hep-ex].

[57] F. V. Ignatov *et al.* (CMD-3), (2023), arXiv:2309.12910 [hep-ex].

[58] S. Borsanyi *et al.*, Nature **593**, 51 (2021), arXiv:2002.12347 [hep-lat].

[59] A. Berlin, N. Blinov, G. Krnjaic, P. Schuster, and N. Toro, Phys. Rev. D **99**, 075001 (2019), arXiv:1807.01730 [hep-ph].

[60] W. Altmannshofer, S. Gori, M. Pospelov, and I. Yavin, Phys. Rev. Lett. **113**, 091801 (2014), arXiv:1406.2332 [hep-ph].

[61] R. Godang (BABAR), EPJ Web Conf. **141**, 02005 (2017), arXiv:1611.07934 [hep-ex].

[62] R. Capdevilla, D. Curtin, Y. Kahn, and G. Krnjaic, JHEP **04**, 129 (2022), arXiv:2112.08377 [hep-ph].

[63] Y. Kaneta and T. Shimomura, PTEP **2017**, 053B04 (2017), arXiv:1701.00156 [hep-ph].

[64] S. Gninenko and D. Gorbunov, Phys. Lett. B **823**, 136739 (2021), arXiv:2007.16098 [hep-ph].

[65] S. N. Gninenko, D. V. Kirpichnikov, M. M. Kirsanov, and N. V. Krasnikov, Phys. Lett. B **796**, 117 (2019), arXiv:1903.07899 [hep-ph].

[66] S. N. Gninenko, D. V. Kirpichnikov, and N. V. Krasnikov, Phys. Rev. D **100**, 035003 (2019), arXiv:1810.06856 [hep-ph].

[67] S. Gninenko, S. Kovalenko, S. Kuleshov, V. E. Lyubovitskij, and A. S. Zhevlakov, Phys. Rev. D **98**, 015007 (2018), arXiv:1804.05550 [hep-ph].

[68] S. N. Gninenko and N. V. Krasnikov (NA64), Phys. Rev. D **106**, 015003 (2022), arXiv:2202.04410 [hep-ph].

[69] B. Radics, L. Molina-Bueno, L. Fields., H. Sieber, and P. Crivelli, Eur. Phys. J. C **83**, 775 (2023), arXiv:2306.07405 [hep-ex].

[70] A. Ariga, R. Balkin, I. Galon, E. Kajomovitz, and Y. Soreq, Phys. Rev. D **109**, 035003 (2024), arXiv:2305.03102 [hep-ph].